EasyChair Preprint

№ 1795

Plasma Treatment in-Water Processes of Sugarcane Bagasse

Muh. Firdan Nurdin, Novriany Amaliyah and
Andi Erwin Eka Putra

October 31, 2019

Plasma Treatment in-Water Processes of Sugarcane Bagasse

Muh. Firdan Nurdin[1*], Novrianty Amaliah[1], Andi Erwin Eka Putra[1]

1 Department of Mechanical Engineering, Hasanuddin University

* Corresponding author: firdanfino@gmail.com

Abstract

Sugarcane (Saccharum officinarum L.) is an indispensable plant, representing most of the cultivated plants throughout the world. Sugarcane is processed to produce crystalline sugar and bioethanol. The treatment process produces sugarcane bagasse waste. Sugarcane bagasse waste can be utilized through some treatment. In this study, Plasma Treatment (PT) in-Water treatment was applied to sugarcane bagasse to investigated the glucose concentrates and by-products. PT in-water energy input parameters were 320, 340, and 400 W with an irradiation time of 1, 2.5 and 5 minutes. Sugarcane bagasse after treatment and by-products were tested using the Nelson Somogyi method to determine glucose percentage and characterized using Fourier Transform Infrared Spectroscopy (FT-IR), Scanning Electron Microscope (SEM) and Image-J software. The results showed that the percentage of glucose in sugarcane bagasse decreased from 0.028% to 0.00023% at 400 W energy input, the irradiation time of 5 minutes. the by-product resulted in cellulose nanoparticles which had an average diameter from 276.14 to 105.78 nm at each energy input variation.

1. Introduction

Sugarcane (*Saccharum officinarum L.*) is an indispensable crop, representing a significant proportion of cultivated crops worldwide. Its annual global production of ~1.6 billion tons generates several hundred million metric tons of bagasse or remaining fiber after the extraction of the sugar-bearing juice[1]. Bagasse is composed of up to 70% holocellulose, which is represented by high tensile strength crystalline cellulose with intervening amorphous regions gathered into bundles of microfibrils embedded in an amorphous matrix of hemicellulose and further crosslinked lignin. Small amounts of

pectin, extractives, and ashes also are included in the biomass composition[2]. United Nations data estimates up to 493 million metric tons of bagasse generates globally from the sugar industry [3]. Sugarcane bagasse contains cellulose around 39.5% - 45.7%, hemicellulose around 25.6% - 29.6%, lignin around 2.3% - 10.5%, minerals around 2.3% - 10.5% and ash around 1.1% - 6% [4]. Cellulose is composed of ß(1-4) diequatorially linked D-glucose molecules that associate through strong hydrogen bonding and pack together in a hierarchical fashion. Within the plant cell wall, other polysaccharides are associated with cellulose, such as hemicelluloses, pectin, and lignin[5]. For sugarcane bagasse, there is a pre-treatment process using alkaline solutions such as NaOH or H_2SO_4 to the breakdown of the cellulose network in bagasse[6].

Plasma processing has inherent advantages in the production of advanced materials such as the wide field of nanomaterials. At high temperatures chemically reactive species formed in the plasma through the vapor phase, the reaction may accelerate chemical reactions for the production of nanoparticles[7]. Plasma technology methods were implemented to produce nanomaterials such as nano-diamond, nanocarbon and nanoparticles[8]–[10]. Nanometer or micrometer-sized particles can be formed by plasma technology. Plasma is normal electron-ion with an additional highly charged component of massive particulates and/or dust grains[11].

The high efficiency of plasma is a result of its high temperature and presence of reactive species such as electrons, ions, radicals, etc that enhance chemical reactions[12]. The radicals have an important role in the deconstruction of a biomass lignocellulosic matrix, particularly degrading the lignin with good efficiency[13]. In contrary to most plasma methods, plasma microwaves can use a magnetron similar to that used in other industrial applications, e.g. drying or food processing. They are relatively cheap and have a simple and compact construction similar to the domestic microwave oven[14]. Plasma technology-assisted chemical pretreatments were implemented to increase sugar content in sugarcane bagasse[15].

The technology treatment for sugarcane bagasse currently still requires several chemical methods. Therefore, the purpose of this research is to investigate the *Plasma Treatment in-Water Processes of Sugarcane Bagasse.*

2. Material and Methods

2.1. Material

The sugarcane bagasse was obtained from PT. Takalar Sugar Factory. Sugarcane bagasse was cleaned and dried by sun for 3 days until a low humidity level. Then it

was sifted by 10, 20 and 45 mesh to obtain the uniform size range is 3 – 5 mm. The sugarcane bagasse sample is shown in figure 1.

Fig. 1. Sugarcane Bagasse

2.2. Treatment Process

2.2.1. Plasma Treatment In-Water

In PT in-Water method, Sample was prepared at 10 % w/v weight of the sugarcane bagasse to the volume of distilled water. The sample was put into the reactor by adding distilled water. It was treated by microwave plasma with a variation of time in 1 minute, 2.5 minutes, 5 minutes and energy input at 320, 360 and 400 W. The percentage glucose of the sample was tested using the Nelson Somogyi method. Characterization by-product was conducted using FTIR and SEM. The Schematic Apparatus of PT in-Water has shown in figure 2.

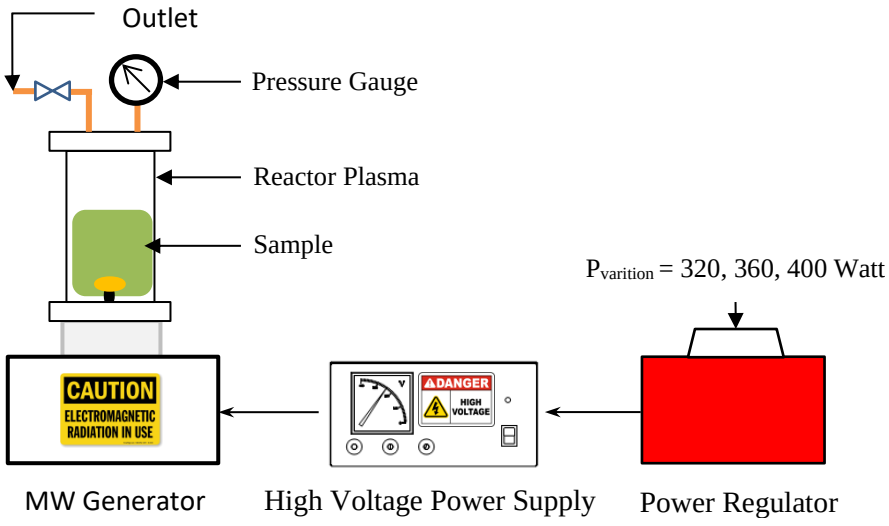

Fig. 2. The Schematic Apparatus of PT in-Water

2.2.2. Nelson Somogyi Method

In this method, Nelson's reagent is used to determine glucose content and then determine the glucose concentration by spectrophotometry. The Nelson reagent is a combination of Nelson A reagents and Nelson B reagents with a volume ratio of 25 : 1 (ml). The color of Nelson's reagent is blue. Reducing sugar (glucose) will reduce oxidizing compounds ($CuSO_4$, $5H_2O$) to red brick deposits (Cu_2O). After adding the Nelson reagent, the sample was warmed up so that it will show the presence of deposits on the bottom of the test tube which is assumed to be the Cu_2O brick-red precipitate in the sample which has a high reducing sugar concentration. In absorption measurement, the wavelength of 540 nm is the maximum wavelength of glucose.

2.2.3. Product Characterization

Scanning electron microscope (SEM) (TM-3000, Hitachi) at 15 kV (voltage acceleration) was used to study the morphology of sugarcane pulp by-products after plasma treatment. Furthermore, the chemical structures of the by-product of sugarcane bagasse were identified by the peak of FTIR characteristics (IRPrestige-21 SHIMADZU). Result and Discussion.

3. Result

The percentage of glucose in sugarcane bagasse before treatment is 0.028%. After treatment by using PT in-Water, the percentage of glucose in sugarcane bagasse was decreased. It was influenced by input power and time treatment of the PT in-Water. The result is shown in figure 3.

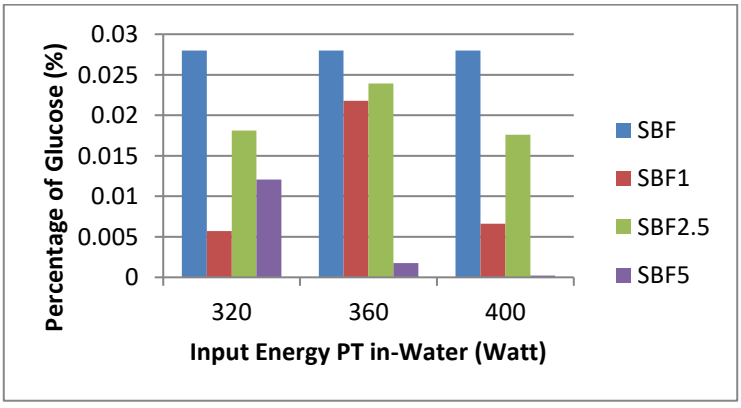

SBF = Sugarcane Bagasse Fiber 1, 2.5, 5 = Variation of treatment time (Min)

Fig. 3. The percentage of glucose to the variation of input energy PT in-Water of each sample.

Decreased glucose levels in the PT in-water process can be influenced by the characteristics of the plasma. Plasma has a very high electron temperature around 10^3~10^4 K so that it is able to produce active species [16], [17]. Active species produced by plasma technology in various liquid phases or Solution Plasma Process (SPP) namely H_2O_2, O, $OH^{\bullet}$, H_α, H_β, O^*, HO_2, $O_3{}^*$, $N_2{}^*$, e^-, $O_2{}^-$, O^-, $O_2{}^+$, e^{-*}, $H^{\bullet}$ which can play a role in the process of decomposition of organic compounds [17]–[19]. S.Nomura, et al have reported that the highest intensity of active species produced during the microwave plasma process is $OH^{\bullet}$ [19]. Baroch, et al have also reported that the production of hydroxyl radicals can occur in the process of in-water plasma treatment through the reaction of radical oxygen with water in the system [15]. The mechanism of active hydroxyl radical formation (equation 4 - 7) [18].

$$e^{-*} + H_2O \rightarrow e^- + OH^{\bullet} + H^{\bullet} \quad (4)$$

$$e^{-*} + O_2 \rightarrow e^- + O(^1D) + O(^3P) \quad (5)$$

$$O(^1D) + H_2O \rightarrow 2OH^{\bullet} \quad (6)$$

$$O(^3P) + H_2O \rightarrow 2OH^{\bullet} \quad (7)$$

Tne one of active species is the active hydroxyl radical ($OH^{\bullet}$) which can effectively abstract cellulose and hydrogen bonds [20], [21]. $OH^{\bullet}$ can extract O-H and C-O bonds in glucose through the transfer of hydrogen $OH^{\bullet}$ to glucose oxygen atoms. This results in the opening of the glucose pyran ring (figure 3) [22]. Therefore, the reduction in glucose levels in sugarcane bagasse after plasma treatment is assumed to be due to the abstraction of hydrogen glucose by active hydroxyl radicals ($OH^{\bullet}$). High reaction temperatures can also accelerate glucose degradation [23].

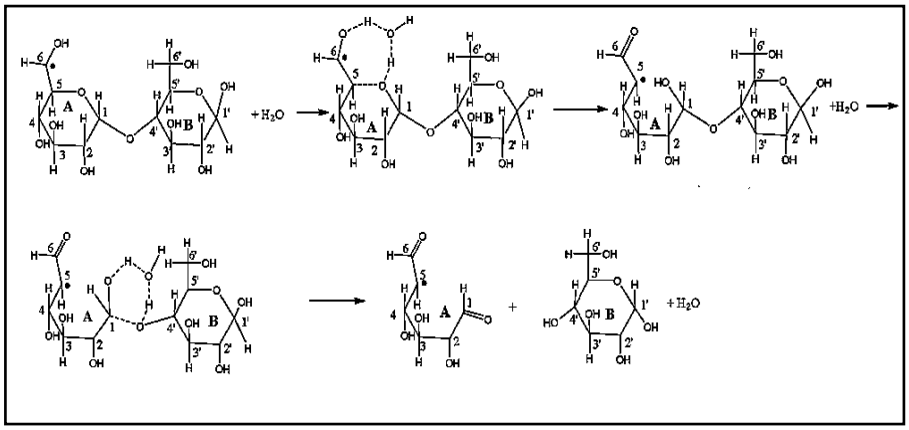

Fig. 3. Opening of the Pyrenean Glucose Ring in the Glucosidic Bond [22].

The distillation water after treatment was tested for glucose content using the nelson Somogyi method (Table 1).

Tabel 1. Measured Glucose in Distilled Water

No.	Sample	Energy Input PT in-Water (W)	Measured Glucose (mg/mL)
			After Treatment
1	DW1	320	0,00055
2	DW2.5	360	0,00134
3	DW5	400	0,001217

DW = Distillated Water 1, 2.5, 5 = Irradiation Time (min)

The table 1 showed measured variations in glucose content in distilled water. The highest measured glucose is at an energy input condition of 400 W and an irradiation time of 5 minutes. It can be assumed that the glucose dissolved in distilled water during the treatment process is due to the active species. One such active species is the hydroxyl radical ($OH^{\bullet}$) which is effectively able to break hydrogen bonds and cellulose structure [20], [21]. Hydroxyl radicals can react with glycosidic bonds to experience the reaction of cutting the polysaccharide chain into glucose monosaccharides (figure 4) [15], [24], [25].

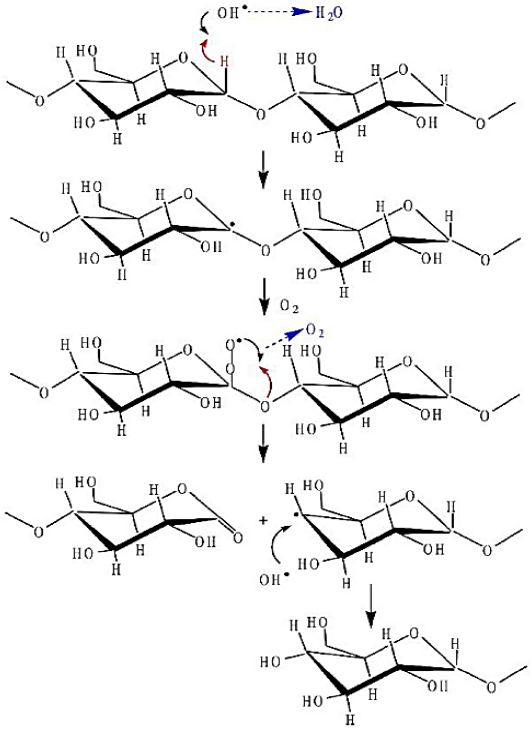

Fig. 4. Scheme Degradation of Glycosidic bond
by oxygen radical species ($OH^{\bullet}$) [25].

Hydroxyl radicals can separate hydrogen atoms in C-1 carbon that form glycosidic bonds into water molecules (H_2O). Subsequently, carbon radicals are formed and react

with oxygen through an oxidation process to form superoxide anions. This results in a cut between α-1.4 glycosidic sugarcane bagasse molecules. Then, carbonyl groups are formed and C-4 carbon radicals react with hydroxyl radicals to produce glucose [25]. The glucose produced will dissolve into water.

The solid materials of by-product were obtained from the dried process of the liquid product was analyzed using FTIR SHIMADZU to identify the functional groups of a compound.

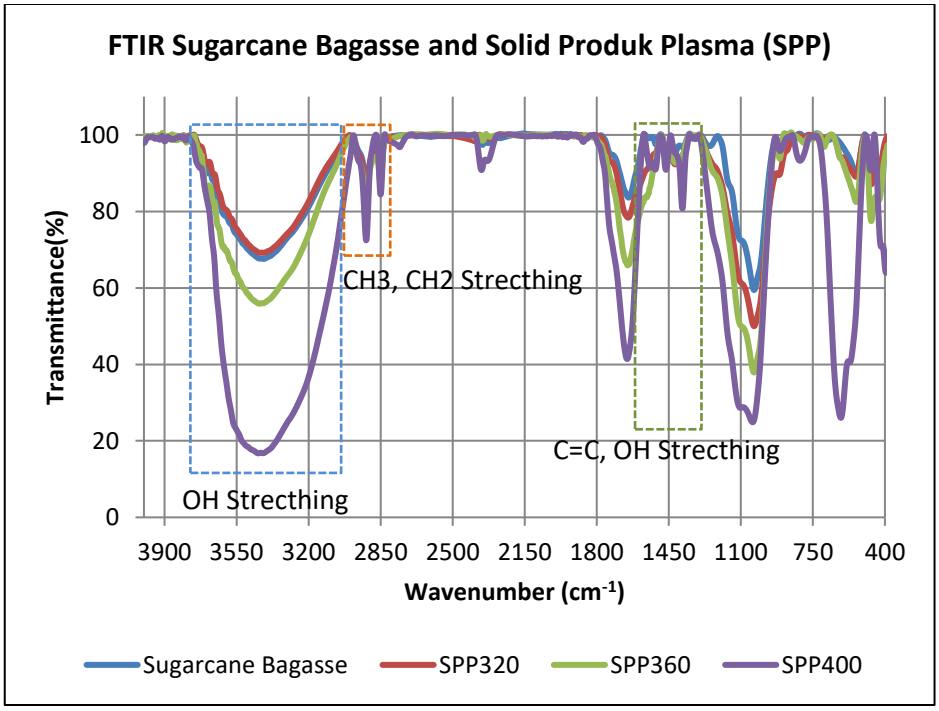

Fig. 5. FTIR of Sugarcane Bagasse and Solid Product Plasma

Figure 5 shows the results of sugarcane bagasse raw material testing before testing Raw Materials (Blue Line) of by-products (Solid Plasma Products / SPP) after assistance with variations in energy input 320, 360, and 400 Watt (SPP320, SPP360, SPP400).

At SPP320 (Red Line), SPP360 (Green Line), and SPP400 (Purple Line) have peaks 3437.15, 3437.15 and 3444.87 cm^{-1}, each of which is identified as a functional O – H stretching group. In cellulose, vibrations of intramolecular hydrogen bonds appear around 3432 cm-1 to 3400 cm-1 [26], [27]. The SPP320, SPP360, and SPP400 have peaks of 2920.23 cm^{-1} and 2850.79 cm^{-1}, which are identified as asymmetric and symmetrical methyl and methylene functional groups. Peaks around 2920 cm^{-1} and 2850 cm^{-1} are related to the asymmetric and symmetrical methyl and methylene groups found in the spectrum of all-fiber components, especially in the cellulose spectrum [27]. The sugarcane

bagasse has a peak of 1730.15 cm^{-1} which is indicated to be a region of the C = C group of lignin and hemicellulose vibrations, but SPP320, SPP360, and SPP400 are not found peaks in that area [28], [29]. SPP320, SPP360, and SPP400 have peaks, 1647.21, 1643.45, and 1653.00 cm^{-1}, which are C = C (Alkene) functional groups identified as deformation or stretching vibrations of the cellulose O-H cellulose group, respectively [30]. In the functional group C = C (Alkene) is also identified as an aromatic region of lignin. In the fingerprint area, peaks in raw materials, SPP 360, SPP 400 namely 1512.19, 1558.48 and 1541.12 cm-1 are indications of $C = C$, $C - O$ stretching or bending vibrations of various groups contained in lignin [27], [31]. SPP360 and SPP400 have peaks of 873.75, and 812.03 cm^{-1} which are indicated to amorphous regions in cellulose [32]. From the results of FTIR analysis on solid plasma products, there are no hemicellulosic bonds but lignin bonds are still present.

Table 2. The Peaks of FTIR of Lignocellulose Biomass [29].

Wavenumbers (cm^{-1})	Chemical groups and vibration modes
3300	v $(O - H)$ in hydroxyl groups (lignin and cellulose)
2880	v $(C - H)$ in methyl and methylene groups (cellulose)
1725	v $(C = O)$ in lignin and hemicellulose
1610 – 1595	v $(C = C)$ of aromatic ring (lignin)
1470	$\delta_a(CH_3)$ in lignin
1360	$\delta(O - H)$ in Cellulosa
1230	v $(C - O - C)$ in phenol-ether bonds of lignin
1160	v $(C = O)$ in aliphatic groups
1030	$C - O$ deforming in secondary alcohol and aliphatic ether

v: stretching, δ: bending, a: asymmetric mode

SEM testing was conducted to determine the morphology of solid product plasma and using *free-software* Imag-J for obtained the average diameter of particles. However, in the analysis of the particles, it has limited analysis according to the smallest scale of the image. The smallest scale size determines the accuracy of the analysis so that it can influence the results of the analysis. The accuracy of particle analysis using Image-J compared with particle measurements with *Particle Size Analyzer* (PSA) is quite good with an average accuracy rate of 88% in the sample. This shows that particle analysis using Image-J is accurate enough to be applied to the results of SEM imaging [33].

SEM Image Threshold Image Outline Image

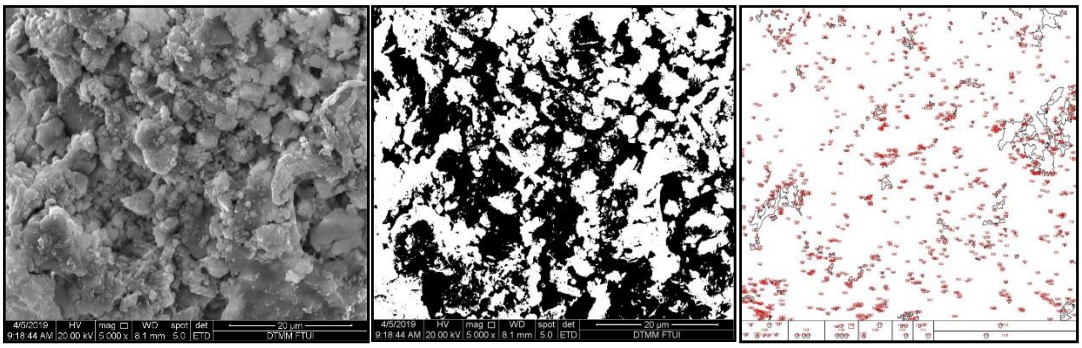

(a)

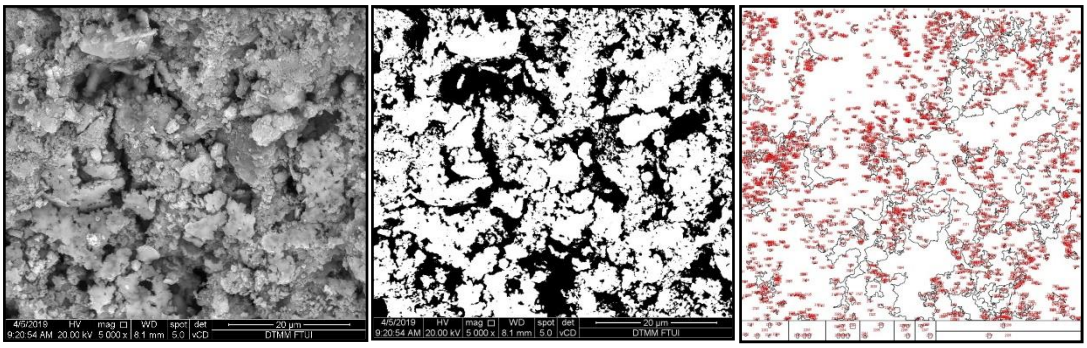

(b)

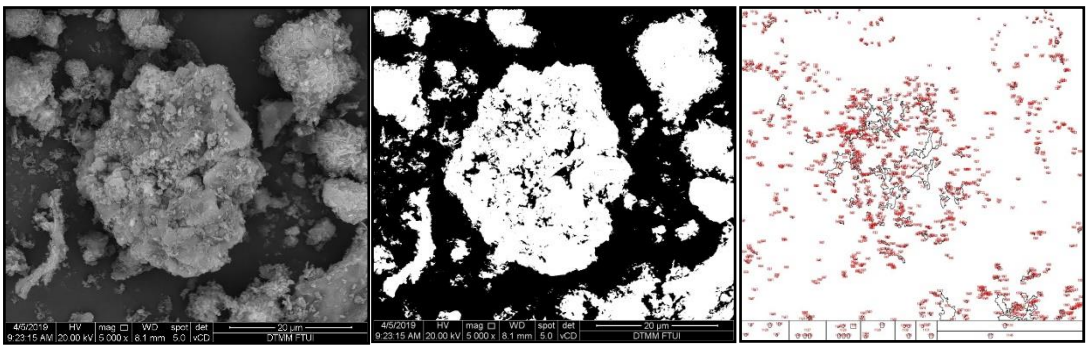

(c)

Fig. 6. SEM Testing Results at Magnification 5000x (a) SM320, (b) SM360, (c) SM400

Figure 6 shows the results of SEM testing for by-products (Solid Material). The image shows the results of the magnification 5000x with reference size is equal to 20 µm. By using ImageJ, the average area and the average diameter of the solid material were obtained. It showed in Table 3.

Table 3. The results of the particle size calculation of the average sample with the magnification 5000x

No.	Samples	The Average Area (nm^2)	The Average Diameter (nm)
1	SM320	257753.23	286.51
2	SM360	346701.50	332.29
3	SM400	239438.93	276.14

The average diameter of each sample meets the criteria of nanomaterial size namely nano-cellulose. The average diameter SM320, SM360, and SM400 were 286.51, 332.29, 276,14 nm, respectively.

SEM Image Threshold Image Outline Image

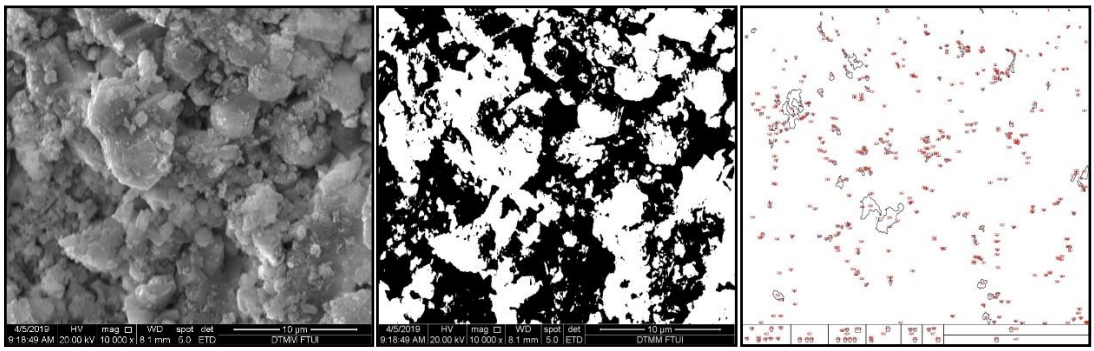

(a)

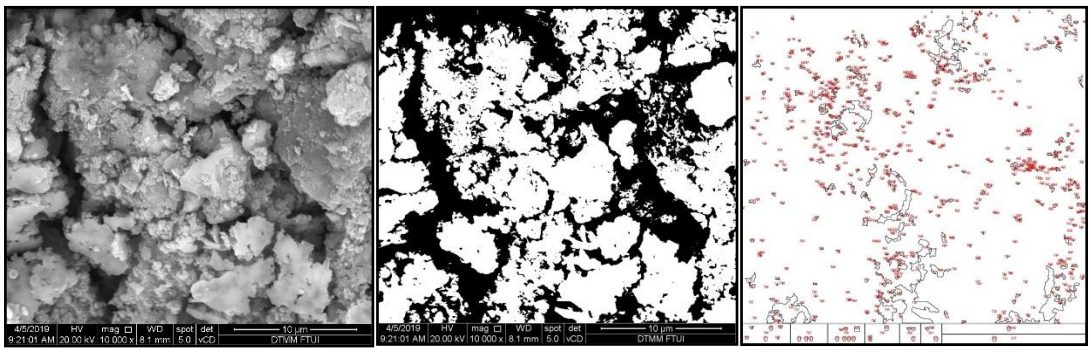

(b)

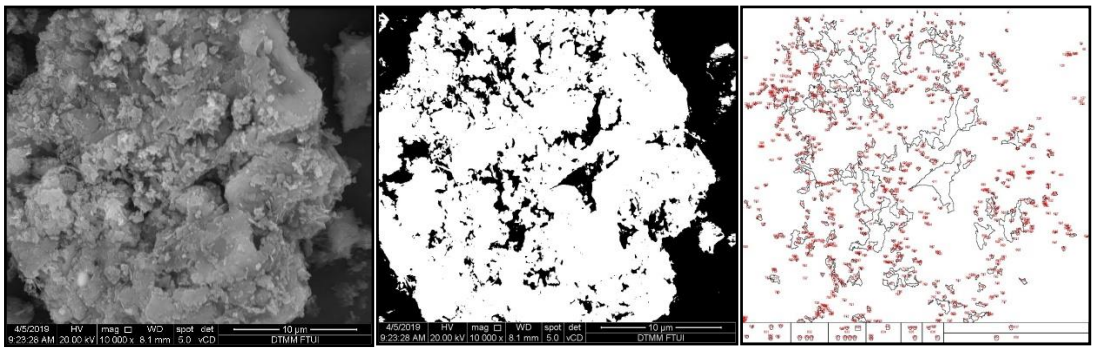

(c)

Fig. 7. SEM Testing Results at Magnification 10000x (a) SM320, (b) SM360, (c) SM400

Figure 7, shows the results of SEM testing for by-products (Solid Material). The image shows the results of the magnification 10000x with reference size is equal to 10 µm. By using ImageJ, the average area and the average diameter of the solid material were obtained. It showed in Table 4.

Table 4. The results of the particle size calculation of the average sample with the magnification 10000x

No.	Samples	The Average Area (nm^2)	The Average Diameter (nm)
1	SM320	130607.13	203.95
2	SM360	103366.58	181.44
3	SM400	133538.71	206.22

The average diameter of each sample meets the criteria of nanomaterial size, namely nano-cellulose. The average diameter SPP320, SPP360, and SPP400 were 203.95, 181.44, 206.22 nm, respectively.

SEM Image Threshold Image Outline Image

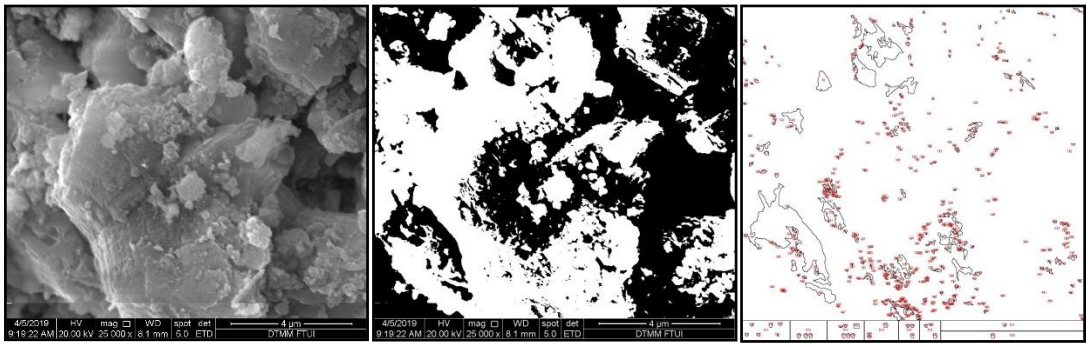

(a)

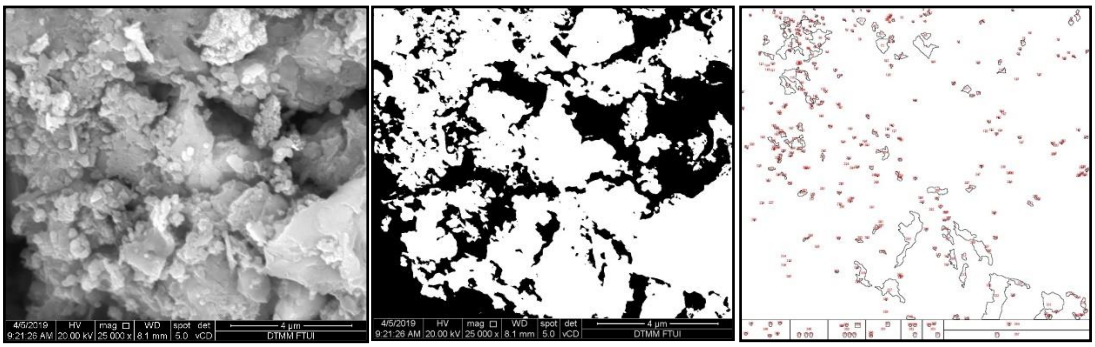

(b)

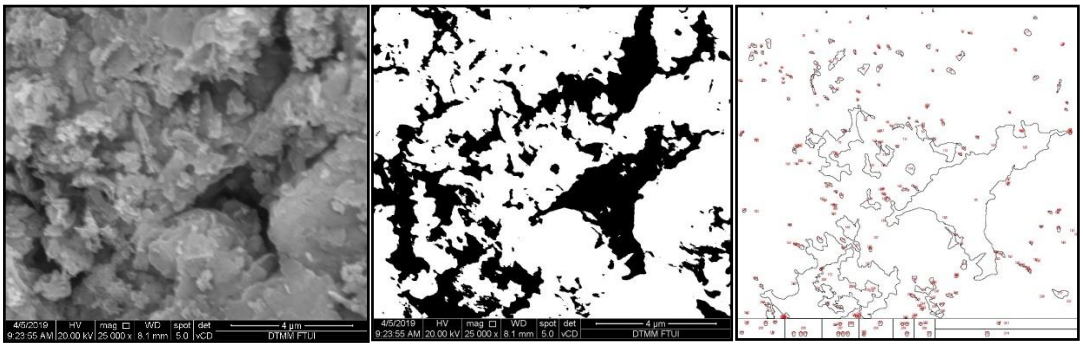

(c)

Fig. 8. SEM Testing Results at Magnification 25000x (a) SPP320, (b) SPP360, (c) SPP400

Figure 8 has shown the results of SEM testing for by-products (Solid Material). The image shows the results of the magnification 25000x with reference size is equal to 4 µm. By using ImageJ, the average area and the average diameter of the solid material were obtained. It showed in Table 5.

Table 5. The results of the particle size calculation of the average sample with the magnification 25000x

No.	Samples	The Average Area (nm^2)	The Average Diameter (nm)
1	SPP320	26714.46	92.24
2	SPP360	35132.82	105.78
3	SPP400	89546.48	168.87

The average diameter of each sample meets the criteria of nanomaterial size, namely nano-cellulose. The average diameter SPP320, SPP360, and SPP400 were 92.24, 105.78, 168.87 nm, respectively.

The average particle diameter of SM320, SM360, and SM400 has obtained in the range between 92.24 to 332.29 nm. Cellulose nanoparticles (CNP) of average particle

diameter ranging from 70 to 365 nm were obtained from cotton through optimizing the synthesis conditions such as the ratio of solvent/nonsolvent, concentrations of the cellulose, and the use of water-in-oil (w/o) microemulsion [34]. Therefore, the solid material (SM320, SM360, and SM400) are CNP.

Cellulose Nanoparticles are having various commercial and biomedical applications. In the agricultural industry, it is mainly used for seed treatment and as a biopesticide in order to fight fungal infections in plants. In winemaking, it can be used as a fining agent and also help to prevent spoilage. In medicine, it is useful as an antibacterial agent, and also assists in the delivery of drugs through the skin [35].

4. Conclusion

The results of this research show that microwave pyrolysis technology is more effective in increasing glucose levels in sugarcane bagasse than Plasma Technology in-Water (PT in-Water). However, the PT in-Water in the treatment of sugarcane bagasse was produced side product in the form of solid materials and was identified using FTIR and SEM as cellulose nanoparticles (CNP).

Reference

[1] R. Hatfield and R. S. Fukushima, “Can Lignin Be Accurately Measured ?,” pp. 832–839, 2005.

[2] S. M. R. Khattab and T. Watanabe, *Policía Nacional Revolucionaria Objetivos del Curso – taller*. Elsevier Inc., 2019.

[3] “UN Energy Statistics Database, 2013.” [Online]. Available: https://unstats.un.org/unsd/energy/edbase.htm.

[4] K. Saha, A. Maharana, J. Sikder, S. Chakraborty, S. Curcio, and E. Drioli, “Continuous production of bioethanol from sugarcane bagasse and downstream purification using membrane integrated bioreactor,” *Catalysis Today*, Elsevier B.V., 2018.

[5] L. J. Gibson, “The hierarchical structure and mechanics of plant materials,” no. August, pp. 2749–2766, 2012.

[6] G. J. de M. Rocha, V. M. Nascimento, A. R. Gonçalves, V. F. N. Silva, and C. Martín, “Influence of mixed sugarcane bagasse samples evaluated by elemental and physical-chemical composition,” *Ind. Crops Prod.*, vol. 64, pp. 52–58, 2015.

[7] S. Samal, “Thermal plasma technology: The prospective future in material processing,” *Journal of Cleaner Production*, vol. 142. Elsevier Ltd, pp. 3131–3150, 2017.

[8] C. H. Nee, M. C. Lee, H. S. Poh, S. L. Yap, T. Y. Tou, and S. S. Yap, “Plasma synthesis of nanodiamonds in ethanol,” *Compos. Part B Eng.*, vol. 162, pp. 162–166, 2019.

[9] D. Mariotti, J. Patel, V. Švrček, and P. Maguire, “Plasma-liquid interactions at atmospheric pressure for nanomaterials synthesis and surface engineering,” *Plasma Process. Polym.*, vol. 9, no. 11–12, pp. 1074–1085, 2012.

[10] X. Tu and J. C. Whitehead, “Plasma dry reforming of methane in an atmospheric pressure AC gliding arc discharge: Co-generation of syngas and carbon nanomaterials,” *Int. J. Hydrogen Energy*, vol. 39, no. 18, pp. 9658–9669, 2014.

[11] T. Vacková, P. Špatenka, and S. Balakrishna, “Plasma Treatment of Powders and Fibers,” in *Non-Thermal Plasma Technology for Polymeric Materials*, 2019, pp. 193–210.

[12] P. Jamróz, W. Kordylewski, and M. Wnukowski, “Microwave plasma application in decomposition and steam reforming of model tar compounds,” *Fuel Process. Technol.*, vol. 169, no. July 2017, pp. 1–14, 2018.

[13] M. T. B. Pimenta *et al.*, “Hydrothermal and Atmospheric Pressure Microplasma Pretreatment Processes of Sugarcane Bagasse,” no. FEBRUARY, pp. 1–9, 2010.

[14] G. J. Van Rooij, D. C. M. Van Den Bekerom, N. Den Harder, and T. Minea, “Taming microwave plasma to beat thermodynamics in CO 2 dissociation,” *Faraday Discuss.*, vol. 00, pp. 1–16, 2015.

[15] I. Prasertsung, P. Chutinate, A. Watthanaphanit, N. Saito, and S. Damrongsakkul, “Conversion of cellulose into reducing sugar by solution plasma process (SPP),”

Carbohydr. Polym., vol. 172, pp. 230–236, 2017.

[16] X. Chen, Y. Cheng, T. Li, and Y. Cheng, "Characteristics and applications of plasma-assisted chemical processes and reactors," *Current Opinion in Chemical Engineering*, vol. 17. Elsevier Ltd, pp. 68–77, 2017.

[17] P. Baroch, V. Anita, N. Saito, and O. Takai, "Bipolar pulsed electrical discharge for the decomposition of organic compounds in water," vol. 66, pp. 294–299, 2008.

[18] S. Horikoshi and N. Serpone, "In-liquid plasma: A novel tool in the fabrication of nanomaterials and in the treatment of wastewaters," *RSC Adv.*, vol. 7, no. 75, pp. 47196–47218, 2017.

[19] S. Nomura *et al.*, "Discharge characteristics of microwave and high-frequency in-liquid plasma in water," *Appl. Phys. Express*, vol. 1, no. 4, pp. 0460021–0460023, 2008.

[20] O. Takai, "Solution plasma processing (SPP)," *Pure Appl. Chem.*, vol. 80, no. 9, pp. 2003–2011, 2008.

[21] L. Gao *et al.*, "Hydroxyl radical-aided thermal pretreatment of algal biomass for enhanced biodegradability," *Biotechnol. Biofuels*, vol. 8, no. 1, pp. 1–11, 2015.

[22] Y. Dai *et al.*, "The mechanism for cleavage of three typical glucosidic bonds induced by hydroxyl free radical," *Carbohydr. Polym.*, vol. 178, no. 29, pp. 34–40, 2017.

[23] Y. Xiong, Z. Zhang, X. Wang, B. Liu, and J. Lin, "Hydrolysis of cellulose in ionic liquids catalyzed by a magnetically-recoverable solid acid catalyst," *Chem. Eng. J.*, vol. 235, pp. 349–355, 2014.

[24] J. Duan and D. L. Kasper, "Oxidative depolymerization of polysaccharides by reactive oxygen/nitrogen species," *Glycobiology*, vol. 21, no. 4. pp. 401–409, 2011.

[25] I. Prasertsung, K. Aroonraj, K. Kamwilaisak, N. Saito, and S. Damrongsakkul, "Production of reducing sugar from cassava starch waste (CSW) using solution plasma process (SPP)," *Carbohydr. Polym.*, vol. 205, no. July 2018, pp. 472–479, 2019.

[26] M. Poletto, H. L. Ornaghi Júnior, and A. J. Zattera, "Native cellulose: Structure, characterization and thermal properties," *Materials (Basel).*, vol. 7, no. 9, pp. 6105–6119, 2014.

[27] M. Poletto, A. J. Zattera, and R. M. C. Santana, "Structural Differences Between Wood Species : Evidence from Chemical Composition, FTIR Spectroscopy, and Thermogravimetric Analysis," 2012.

[28] K. Plermjai, K. Boonyarattanakalin, W. Mekprasart, S. Pavasupree, W. Phoohinkong, and W. Pecharapa, "Extraction and characterization of nanocellulose from sugarcane bagasse by ball-milling-assisted acid hydrolysis," in *AIP Conference Proceedings*, 2018, vol. 2010.

[29] M. Bigan and B. Mutel, "Cold remote plasma modification of wood: Optimization process using experimental design," *Appl. Surf. Sci.*, vol. 453, pp. 423–435, 2018.

[30] H. Kargarzadeh, I. Ahmad, I. Abdullah, A. Dufresne, S. Y. Zainudin, and R. M. Sheltami, "Effects of hydrolysis conditions on the morphology, crystallinity, and thermal stability of cellulose nanocrystals extracted from kenaf bast fibers," *Cellulose*, vol. 19, no. 3, pp. 855–866, 2012.

[31] C. M. Popescu, G. Singurel, M. C. Popescu, C. Vasile, D. S. Argyropoulos, and S. Willför, "Vibrational spectroscopy and X-ray diffraction methods to establish the differences between hardwood and softwood," *Carbohydr. Polym.*, vol. 77, no. 4, pp. 851–857, 2009.

[32] M. Åkerholm, B. Hinterstoisser, and L. Salmén, "Characterization of the crystalline structure of cellulose using static and dynamic FT-IR spectroscopy," *Carbohydr. Res.*, vol. 339, no. 3, pp. 569–578, 2004.

[33] C. Kurniawan, T. B. Waluyo, and Perdamean Sebayang, "Analisis ukuran partikel menggunakan free software Image-J, Serpong.," *Semin. Nas. Fis.*, no. 12-13 Juli 2011, pp. 1–9, 2011.

[34] S. F. Chin, F. B. Jimmy, and S. C. Pang, "Size controlled fabrication of cellulose nanoparticles for drug delivery applications," *J. Drug Deliv. Sci. Technol.*, vol. 43, pp. 262–266, 2018.

[35] Y. Habibi, L. A. Lucia, and O. J. Rojas, "Cellulose Nanocrystals: Chemistry, Self-Assembly, and Applications," *Chem. Rev.*, vol. 110, no. 6, pp. 3479–3500, 2010.